

# EPR Investigation of Local Paramagnetic Centers in Perovskite-Like Crystals

V. N. Voronov\* and E. A. Petrakovskaya

*Kirensky Institute of Physics, Siberian Branch of the Russian Academy of Sciences,  
Akademgorodok 50–38, Krasnoyarsk, 660036 Russia*

\* e-mail: voronov@iph.krasn.ru

Received August 20, 2012; In final form, September 25, 2012

**Abstract**—In  $\text{ScF}_3$  single crystals (pure and doped) as well as in  $\text{Rb}_2\text{KScF}_6$  and  $\text{Rb}_2\text{KDyF}_6$  crystals with a perovskite-like structure, point nanodefects (vacancy in place of trivalent cations) have been found and studied. Electron paramagnetic resonance has been used to investigate local paramagnetic centers that are not detected using X-ray diffraction. The angular dependence of the spectra indicates a local distortion of the cubic symmetry of the crystals. An additional hyperfine structure in the observed spectra is due to the delocalization of electrons over six  $\text{F}^-$  ions forming the first coordination polyhedron around the vacancy. The crystals studied are characterized by a high electron mobility and a high electron velocity, which depends on the impurity. The high mobility of electrons of the cation center can be indirectly responsible for the structural phase transition occurring in the  $\text{ScF}_3$  crystal under uniaxial pressure.

DOI: 10.1134/S1063783413040367

## 1. INTRODUCTION

At present, there is a lot of experimental and theoretical studies concerned with defects in solids [1–15]. In the structure of crystals, the direct observation of point defects is extremely complicated because of their small sizes and low concentrations. In this respect, point defects have usually been detected and investigated predominantly by analyzing their influence on the physical properties of crystals. For example, defects such as anion vacancies with trapped excess electrons, which are responsible in many cases for the color of the crystals ( $F$ -centers), exhibit paramagnetic properties. An  $M$ -center is formed by two electron carriers trapped in neighboring anion vacancies. This center can be regarded as two neighboring  $F$ -centers and represents the simplest of the  $F$ -aggregate states, which were discussed in [6, 10]. An  $R$ -center consists of three neighboring  $F$ -centers. Defects of this type are observed in alkali metal halide crystals [8]. In alkaline-earth metal oxides,  $R$ -centers have different charge states [9]. Defect of this type can be detected using electron paramagnetic resonance (EPR).

In [16], the lattice dynamics of  $\text{ScF}_3$  and the isomorphous compounds  $\text{AlF}_3$ ,  $\text{GaF}_3$ , and  $\text{FeF}_3$  in the cubic phase was calculated in the framework of the *ab initio* model. It was shown that, in the vibrational spectrum of these crystals, there are no imaginary frequencies. The vibrational spectrum of the  $\text{ScF}_3$  crystal has a weakly dispersion branch (between the points  $R$  and  $M$  in the Brillouin zone) with abnormally low frequencies. In this vibrational branch, the triply degenerate mode  $R_5$  at the  $R$  point and the nondegenerate modes in the direc-

tion  $R \rightarrow M$  (including the  $M$  point) correspond to lattice vibrations in which fluorine ions are displaced. It is the condensation of modes of this vibrational branch that is related to structural phase transitions in the majority of halides with the perovskite structure. In the  $\text{ScF}_3$  single crystal, no structural transformations are revealed in the range from room temperature to 4 K. It is also assumed that the phase diagram is sensitive to structural defects and impurities.

Trivalent metal fluorides belong to the family of perovskite-like compounds of the general formula  $\text{ABX}_3$  (Fig. 1), in which there are no cations  $A$ . These compounds have a loose structure, which leads to an increased sensitivity to various impurities and structural defects. The elpasolite-type structure can be obtained from the perovskite structure by replacing every second ion  $B$  ion with the  $B^*$  ion. Different sizes

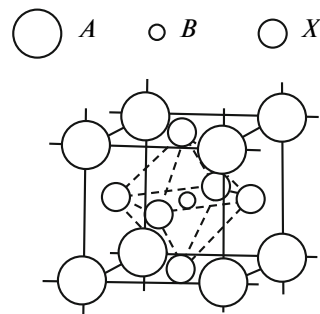


Fig. 1. Unit cell in the perovskite structure.

of the  $B$  and  $B^*$  ions introduce changes into the crystal lattice. The anion coordination polyhedra located around cations  $A$  are distorted in comparison with perovskites; the anion octahedra around the  $B$  and  $B^*$  ions become different in size.

With the aim of studying the nature and specific features of point defects that are responsible for the quality of the crystal and its spectral characteristics, it is proposed, as model objects, to use fluoride compounds with a maximum ionicity of chemical bonds.

## 2. SYNTHESIS OF CRYSTALS

The synthesis of undoped  $\text{ScF}_3$  single crystals and crystals doped with Al, Sb, Ga, Mg, and Fe was performed from solution in the melt. The solvent was sodium fluoride. A mixture of initial reagents containing 40 mol %  $\text{ScF}_3$  was hermetically sealed in a platinum ampoule with a wall thickness of 0.2 mm. The crystallization was carried out using the Bridgman method in a vertical tube furnace with an axial temperature gradient of 10–20 K/cm from the temperature of approximately 1400 K at a rate of  $\sim 1$  mm/h. The X-ray diffraction analysis showed that the obtained crystals corresponded to the structure of the  $\text{ScF}_3$  cubic phase with the unit cell parameter  $a_0 = 4.01$  Å. According to the results of observations in polarized light, all the crystals were optically isotropic [16] (which is characteristic of the cubic symmetry) in the range from room temperature to 120 K.

In this work, we also synthesized single-crystal samples of the  $\text{Rb}_2\text{KFeF}_6$ ,  $\text{Rb}_2\text{KScF}_6$ , and  $\text{Rb}_2\text{KDyF}_6$  compounds with the elpasolite structure. The synthesis of these compounds was performed by sintering stoichiometric compositions with the subsequent melting and crystallization in platinum boats in an argon atmosphere with 10 mol % HF. The axial temperature gradient in the crystallization zone was equal to 10–20 K/cm, and the crystallization rate was 3.5 mm/h. The selected uncontaminated transparent blocks were used for the recrystallization by the Bridgman method without seeds in thin-walled platinum ampoules with a diameter of 10 mm and a wall thickness of 0.2 mm. The axial temperature gradient in the crystallization zone was equal to  $\sim 20$  K/cm, and the crystallization rate was 0.8 mm/h.

## 3. RESULTS OF THE EPR INVESTIGATION

Electron paramagnetic resonance was used as the detection method, which made it possible to check the change of the local symmetry in the pure  $\text{ScF}_3$  crystal and crystals doped with impurities producing the internal pressure in the structure of crystals. Moreover, we investigated the  $A_2BB^*X_6$  perovskite-like crystals with the elpasolite structure. In what follows, in the cases where the electrons responsible for paramagnetic absorption are localized in the material on

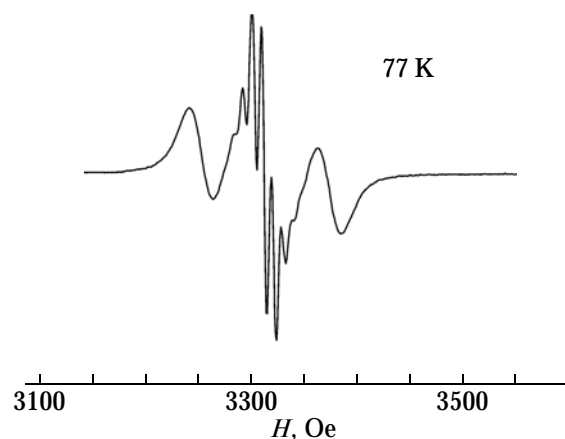


Fig. 2. EPR spectrum of the  $\text{ScF}_3$  single crystal doped with Ga.

defects or impurities, we will use the term “paramagnetic center.” If several unpaired electrons are localized on the paramagnetic center, their interaction with the non-cubic crystal field usually leads to an additional splitting of the energy levels. In this case, we speak about the fine structure of the EPR spectrum. The number of fine structure lines is equal to  $2S$ , where  $S$  is the effective spin of the paramagnetic center. The interaction of unpaired electrons of the paramagnetic ion with the nuclear spin leads to an additional splitting of spectral lines, i.e., the hyperfine structure. The interaction with nuclei of the neighboring ions of the crystal is referred to as the additional hyperfine interaction. Electron paramagnetic resonance provides answers to the questions regarding the degree and character of delocalization of an unpaired electron and its interaction with other electrons of the system. The EPR investigations were performed on an Elexys E580 (Bruker) spectrometer and an SE/X-2544 spectrometer in the temperature range from 293 to 77 K.

We studied pure  $\text{ScF}_3$  single crystals and  $\text{ScF}_3$  crystals doped with Ga and Fe. In addition, we investigated  $\text{Rb}_2\text{KFeF}_6$ ,  $\text{Rb}_2\text{KScF}_6$ , and  $\text{Rb}_2\text{KDyF}_6$  single crystals with the elpasolite structure. An example of the EPR spectrum measured for the Ga-doped  $\text{ScF}_3$  single crystal at a temperature of 77 K is shown Fig. 2.

It can be seen from this figure that, on the central line of the spectrum ( $g = 1.998$ ), there is an additional hyperfine structure (AHFS) consisting of seven components with a splitting of 8 Oe due to the delocalization of electrons over six fluorine ions with the nuclear spin  $I = 1/2$ . A similar spectrum is also observed in the  $\text{ScF}_3$  single crystal without impurities (Fig. 3).

Figure 4 shows the angular dependence of the spectrum of the Ga-doped  $\text{ScF}_3$  single crystal in the (100) plane at 293 K.

As can be seen from the angular dependence, the EPR spectrum belongs to two paramagnetic centers in a distorted cubic position and consists of two triplets.

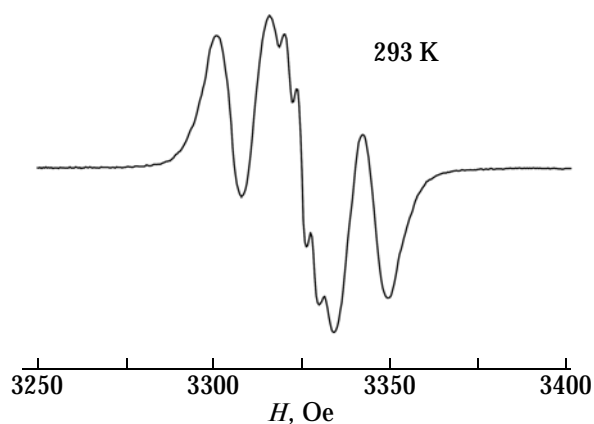


Fig. 3. EPR spectrum of the undoped  $\text{ScF}_3$  single crystal.

The maximum distance between the side components of the triplet is equal to 120 Oe, when the direction of the magnetic field coincides with the distortion axis of the position, and 60 Oe in the direction perpendicular to the distortion axis (Fig. 4a). In the intermediate position ( $45^\circ$ ), the lines merge together into a single broadened line (Fig. 4b). For the undoped single crystal, the angular dependence exhibits a similar behavior with the distance between the AHFS components of 4 Oe. An analysis of the angular dependence of the EPR spectrum shows that the distortion axes for each of these triplets are mutually perpendicular: the maximum splitting of one triplet is accompanied by the splitting of the other triplet, which is approximately two times smaller. Upon rotation through  $90^\circ$ , they change places. The maximum splitting of the triplet is 90 Oe.

The  $\text{ScF}_3$  single crystal doped with iron is characterized by a more complex EPR spectrum (Fig. 5). In this spectrum, there are three clearly seen lines, each consisting of seven slightly overlapping AHFS components. The central line has the  $g$ -factor equal to 1.998. The observed angular change in the positions of these lines indicates a local distortion of the cubic symmetry around this center. The splitting of the spectrum has a maximum value of 217 Oe when the magnetic field is oriented along the distortion axis (Fig. 5a), and the spectral width decreases in the direction perpendicular to the distortion axis (Fig. 5b).

The distance between the neighboring AHFS components is equal to 19–17 Oe. In this case, unlike the two spectra considered above, the delocalization of electrons of the paramagnetic center over six fluorine ions manifests itself for all lines of the triplet. The electron delocalization is especially pronounced for the central line and partially overlaps in the side components. On each side of the spectrum, there are two seven-component transitions with a significantly weaker intensity. Their position does not depend on the orientation of the crystal, and the constant of the additional hyperfine interaction is equal to 13 Oe. The observed spectrum resembles the EPR spectrum of

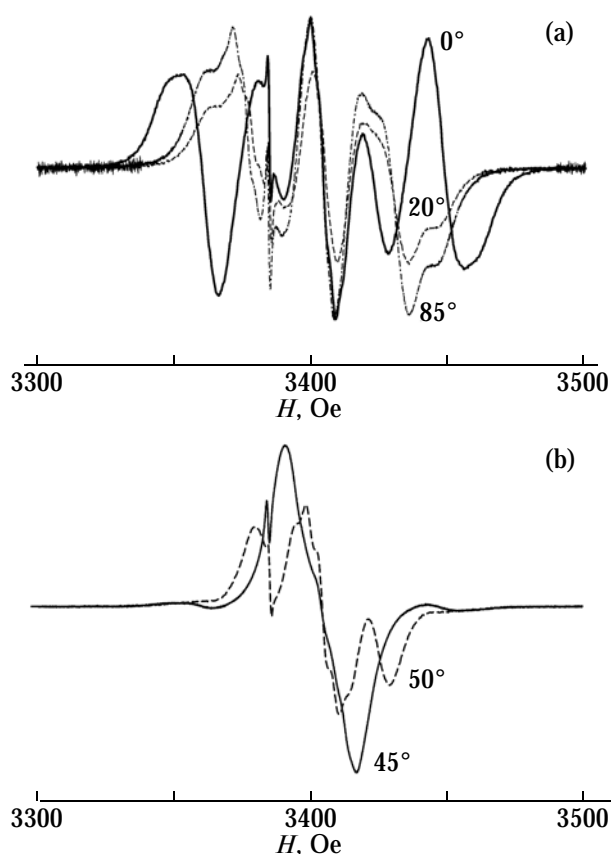
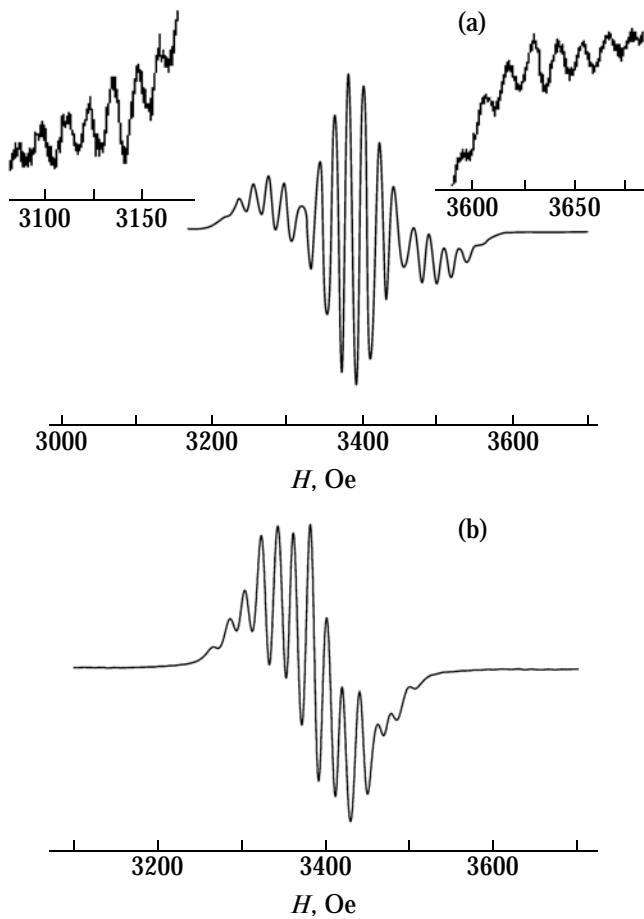


Fig. 4. Angular dependences of the EPR spectrum of the  $\text{ScF}_3$  single crystal doped with Ga: (a) examples of spectra with the highest resolution of the lines (near the parallel and perpendicular orientations of the magnetic field with respect to the axes of the distortion of the octahedron) and (b) examples of spectra with the lowest resolution of the lines (near the  $45^\circ$  orientation).

color centers in  $\text{BaF}_2$  [15], but the structure, in this case, differs from our variant by the value of the electron spin of the defect center. The side components with a substantially lower intensity (insets to Fig. 5a) also arise in our case, probably, due to the interaction of one of the electrons with the Sc nucleus, which has the nuclear spin  $I = 7/2$ .

The EPR spectrum of the  $\text{Rb}_2\text{KScF}_6$  single crystal (Fig. 6a) is similar to the spectrum of the  $\text{ScF}_3$  single crystal doped with iron (Fig. 5). In the EPR spectrum, AHFS is observed for three components; however, there is a difference.

In the central part of the spectrum ( $g = 1.98$ ), there are lines with  $g = 1.97$  and  $1.99$  (Fig. 6b), which can be assigned to the point defects associated with a single electron. On these lines, there is no AHFS. Most likely, we are dealing here with surface defects that are not related to fluorine octahedra. The angular change of the positions of the spectral lines indicates a local distortion of the cubic symmetry in the vicinity of these centers. The maximum distance between the side lines of the triplet is  $D = 248$  Oe. The distance



**Fig. 5.** EPR spectra of the iron-doped  $\text{ScF}_3$  single crystal in the magnetic fields oriented (a) parallel and (b) perpendicular to the distortion axis. The insets show the wings of the spectrum on an enlarged scale.

between the AHFS components is  $a = 18.23$  Oe. As is the case with iron in  $\text{ScF}_3$ , very weak side AHFS components are observed in the spectrum (in the high-field region), which probably can also be attributed to the nearest scandium atom.

The EPR spectrum of the  $\text{Rb}_2\text{KDyF}_6$  single crystal is shown in Fig. 7. The observed spectrum indicates that the structure of the defect in this crystal differs from the previous variants. Upon rotation of the crystal through an angle of  $20^\circ$  from this position, the side components almost completely disappear.

The position of the central line ( $g = 1.99$ ) coincides with one of the doublet lines in the scandium elpasolite. During the rotation of the crystal, the position of the central line changes insignificantly. The maximum distance between the extreme components is equal to 612 Oe. No AHFS is observed in the spectrum; quite possibly, it is simply not resolved. The structure of the defect requires further refinement.

The spectrum of the  $\text{Rb}_2\text{KFeF}_6$  single crystal with an excess ( $\approx 5$  at %) of iron (brown sample) is shown in

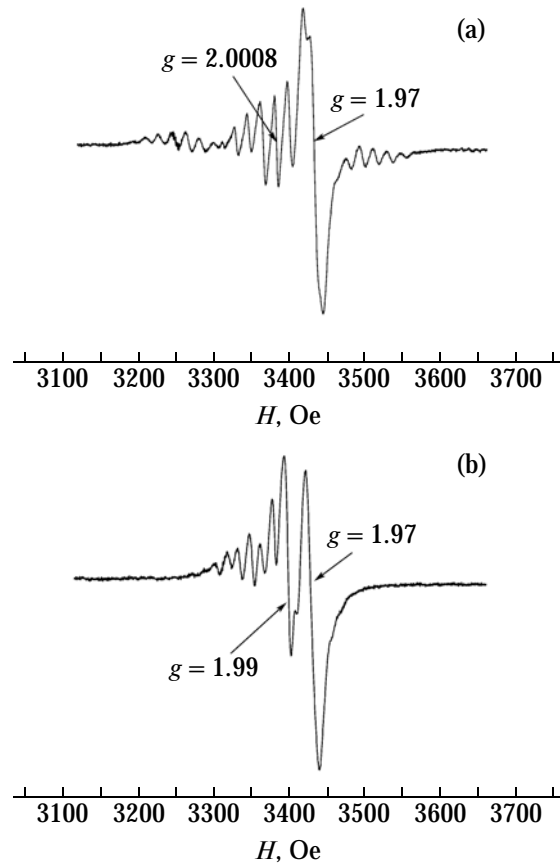


**Fig. 6.** (a) EPR spectrum of the  $\text{Rb}_2\text{KScF}_6$  single crystal and (b) angular change of the positions of the spectral lines.

Fig. 8. The spectrum consists of the line  $g = 2.04$  with a width of 602 Oe, which corresponds to the presence of  $\text{Fe}^{3+}$  in the elpasolite structure. This excess of iron introduced into the crystal during the synthesis provides a sufficient amount of paramagnetic centers in the crystal for the dipole interaction between them, which leads to a broadening of the resonance line. The temperature

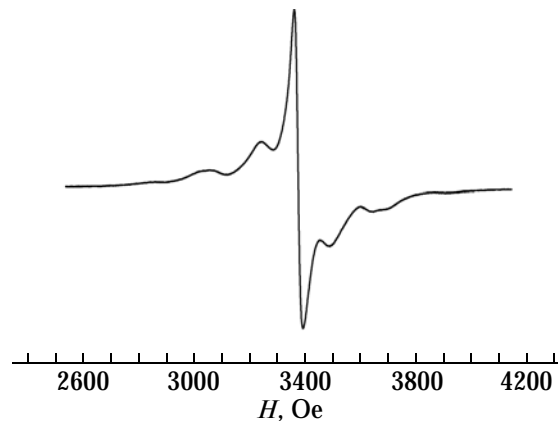


**Fig. 7.** EPR spectrum of the  $\text{Rb}_2\text{KDyF}_6$  single crystal.

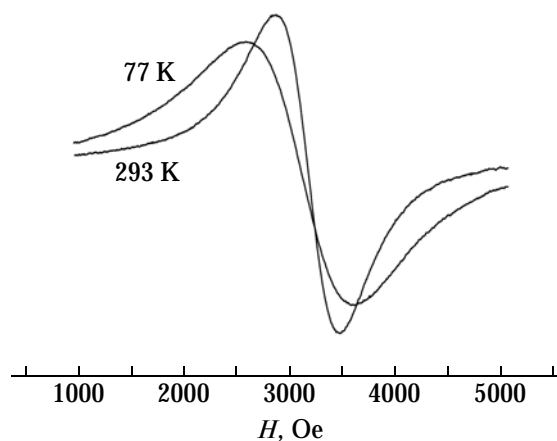


Fig. 8. EPR spectrum of the  $\text{Rb}_2\text{KFeF}_6$  single crystal.

behavior of the spectrum corresponds to the paramagnetic state of iron, although the intensity decreases with a decrease in the temperature. The magnetization equal to the area under the resonance line increases because of the line broadening. This effect is associated with the inhomogeneity of the dipole contribution.

The EPR spectrum of the  $\text{Rb}_2\text{KFeF}_6$  single crystal doped with iron (3 at %) (pink sample) consists of the line  $g = 2.04$  with a width of 680 Oe, which is similar to the line observed for the brown sample. A slight increase in the intensity of the spectrum with decreasing temperature also corresponds to the paramagnetic state. In contrast to  $\text{ScF}_3$ , this crystal does not exhibit lines that can be attributed to defect centers. Although the intensity for the second composition is relatively weak, there is a possibility of overlapping the spectra.

The elpasolite samples are very sensitive to external influences and their environment; moreover, they have the ability to absorb moisture. A few months after the first measurements, the EPR spectra were recorded again. For the  $\text{Rb}_2\text{KFeF}_6$  crystal, the results were reproduced; however, the compounds with dysprosium and scandium did not give spectra at all. After heating of the crystals in a furnace to remove moisture for 8 h at temperatures of 363 and 400 K for the  $\text{Rb}_2\text{KScF}_6$  and  $\text{Rb}_2\text{KDyF}_6$  crystals, respectively, the EPR spectra were still not observed. Furthermore, the EPR experiment was performed on crystals annealed at 473 K. Unfortunately, this experiment also did not give result for the  $\text{Rb}_2\text{KDyF}_6$  crystal. As regards the  $\text{Rb}_2\text{KScF}_6$  crystal, the detected signal was very weak. For the  $\text{ScF}_3$  crystal, the spectrum remained unchanged. The X-ray diffraction analysis did not reveal destruction of the structure in the  $\text{Rb}_2\text{KScF}_6$  and  $\text{Rb}_2\text{KFeF}_6$  crystals. Therefore, in the  $\text{Rb}_2\text{KScF}_6$  crystal, defects were located on the surface. In the  $\text{Rb}_2\text{KDyF}_6$  compound, the crystal structure was completely destroyed.

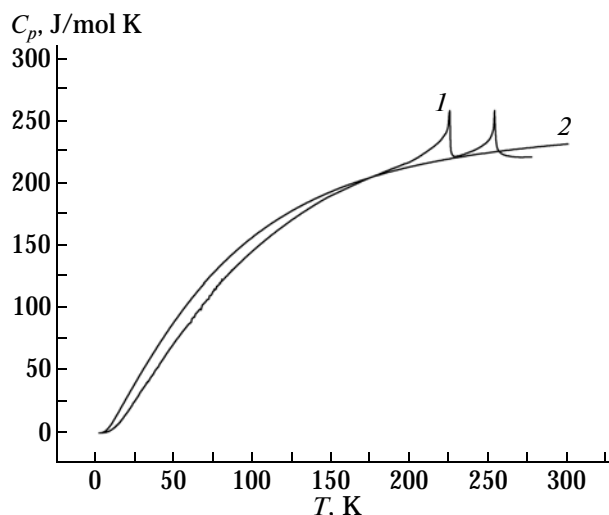


Fig. 9. (1) Experimental and (2) theoretical temperature dependences of the isobaric heat capacity of the  $\text{Rb}_2\text{KScF}_6$  single crystal.

#### 4. CALCULATION OF THE GIBBS ENERGY

Dislocations and interfaces always increase the free energy of the crystal, whereas the introduction of some amount of point defects into the crystal (predominantly, perfect) decreases the free energy to a minimum. Using the experimental temperature dependence of the heat capacity of the  $\text{Rb}_2\text{KScF}_6$  single crystal [17], we constructed a theoretical curve (Fig. 9) and, from it, calculated the Gibbs free energy  $\Delta G = 43165.5 - 315.56T$  [J/mol], where  $T$  is the temperature in degrees Kelvin.

The dependence of the heat capacity  $C_p$  on the temperature  $T$  was calculated using the polynomial approximation to a third-degree polynomial. Then, knowing the dependence  $C_p(T)$ , we calculated the change in the Gibbs free energy  $\Delta G$  according to the following formulas:

$$\Delta G = \Delta H - T\Delta S, \quad (1)$$

$$\Delta S = \int_{T_1}^{T_2} \frac{C_p}{T} dT, \quad (2)$$

$$\Delta H(p = \text{const}) = \int_{T_1}^{T_2} C_p(T) dT. \quad (3)$$

In the framework of the *ab initio* model of an ionic crystal with inclusion of the dipole and quadrupole polarizabilities of the ions [18], we calculated the lattice dynamics of the  $\text{Rb}_2\text{KScF}_6$  crystal in the low-temperature monoclinic phase with symmetry space group  $P2_1/n$ . Based on these calculations, we found the phonon density of states (Fig. 10), which, in turn, was used to calculate the temperature dependence of

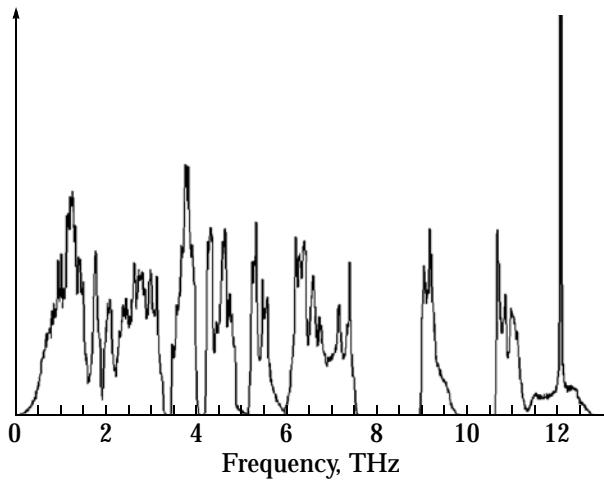


Fig. 10. Phonon density of states for the  $\text{Rb}_2\text{KSrF}_6$  single crystal.

the lattice heat capacity of the studied compound. The heat capacity at each temperature was calculated according to the formula

$$C_v = nk_B \int_0^\infty \left( \frac{\hbar\omega}{k_B T} \right)^2 \frac{e^{\hbar\omega/k_B T}}{(e^{\hbar\omega/k_B T} - 1)^2} g(\omega) d\omega. \quad (4)$$

In the theoretical calculation, we obtained the following value of the Gibbs energy:  $\Delta G = 44507.5 - 352.3T$  [J/mol]. The Gibbs energies obtained at a temperature of 277 K for crystals with defects and without them are  $\Delta G = -44244.62$  and  $-53079.60$  J/mol, respectively. Therefore, in the  $\text{Rb}_2\text{KScF}_6$  elpasolite, surface defects dominate because of the increase in the free energy due to the introduction of defects into the crystal. This is consistent with our experiment, because the  $\text{Rb}_2\text{KScF}_6$  crystal has a sensitive surface.

## 5. DISCUSSION OF THE RESULTS

We assume that, in the  $\text{ScF}_3$  single crystals doped with Ga and in the pure crystal without impurities, there are two  $R$ -centers (Fig. 11). In the EPR spectra of the single crystals doped with Ga and Fe (Figs. 2 and 5), as well as in the pure  $\text{ScF}_3$  crystal (Fig. 3), we observe seven characteristic AHFS lines, which indicate a relation with six  $\text{F}^-$  ions. The fact that there exists a multi-component spectrum due to the electron delocalization over six  $\text{F}^-$  ions suggests that the rate of delocalization, i.e., the frequency of spin transitions from one position to another, is considerably greater than the distance between the AHFS components expressed in terms of a frequency. These crystals are characterized by a high electron mobility and a high electron velocity. For the Ga-doped sample and the pure crystal, the distances between the lines of splitting are 8 and 4 Oe, respectively; for the crystal containing the Fe impurity, this distance is 19 Oe. Therefore, in this case, the rate of

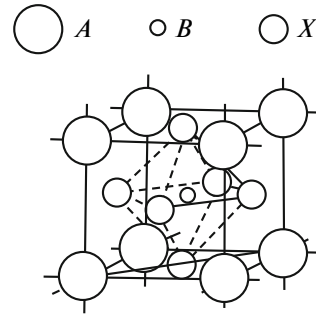


Fig. 11. Drawing of the  $R$ -center in the perovskite structure on the octahedron face bounded by solid lines.

delocalization of electrons has a maximum value. For this reason, probably, AHFS was observed in the first two cases only for the central transition at 77 K. Since the spin of the electron is indivisible, the delocalization of an unpaired electron in the form of a spin-density distribution over the molecule can take place only in the cases where the frequency of spin transitions is significantly higher than the frequencies used in our method of measurement. Based on the data available in the literature [19], the electron delocalization occurs with a frequency in the interval from  $10^{14}$  to  $10^6$   $\text{s}^{-1}$ . The electromagnetic field acting on the sample varies with a frequency of  $10^{10}$   $\text{s}^{-1}$ . Consequently, the delocalization of electrons in the presence of AHFS should be observed in the interval from  $10^{14}$  to  $10^{11}$   $\text{s}^{-1}$ .

The observed angular dependences of the spectra for the single crystals indicate local distortions of the crystal symmetry that are not revealed by X-ray diffraction. The distortion of the cubic structure, according to our results, is associated with the compression or extension of the octahedral positions in the [100] direction. Since we observe two centers with mutually perpendicular axes of distortion of the octahedra, it can be concluded that the octahedra with defect centers are rotated relative to each other locally, so that the cubic structure in general is retained. The results of the investigation of the phase transitions in this crystal under hydrostatic pressure [16] showed the occurrence of this rotation on the scale of the whole crystal and the instability of the cubic phase.

The structure of the  $\text{Rb}_2\text{KScF}_6$  single crystal contains defect centers with  $g = 1.99$ , as is evidenced by the EPR spectrum (Fig. 6). All the lines of the spectrum have an additional hyperfine structure of seven components on each line of the triplet. This structure is determined by the delocalization of three electrons over six fluorine ions. The distance between the components (18 Oe) in the spectrum of  $\text{Rb}_2\text{KScF}_6$  is slightly shorter than that of  $\text{Rb}_2\text{KFeF}_6$  (19 Oe). This fact suggests that the crystal is characterized by a high electron mobility. The observed angular change in the position of the triplet lines indicates a local distortion of the cubic symmetry in the vicinity of this center.

From a comparison of the angular dependences of the spectra for  $\text{Rb}_2\text{KFeF}_6$  and  $\text{ScF}_3$ , as judged from the value of the maximum splitting of the spectrum, we can argue that the distortions of the local symmetry of defect centers located in fluorine octahedra have close values (248 and 217 Oe).

Figure 7 shows the spectrum of the  $\text{Rb}_2\text{KDyF}_6$  single crystal in the form of a narrow line for an angle equal to  $0^\circ$ . The angular dependence of the spectra ( $45^\circ$ ,  $90^\circ$ ) coincides with the angular dependence for the  $\text{ScF}_3$  single crystal (Fig. 4). The only difference is in the intensity of the central line, which overlaps the side components with a deviation from  $0^\circ$  for  $\text{Rb}_2\text{KDyF}_6$ . During the rotation of the single crystal, the positions of the side components change and, at  $90^\circ$ , coincide with those of the spectrum at  $0^\circ$ . This occurs as a result of the local distortion of the structure in the presence of two defects with perpendicular orientations and also additional defects with spin  $1/2$ . The distance between the components with the maximum splitting (corresponding to the orientation of the magnetic field along the distortion axis) for this crystal has a maximum value of 612 Oe, which indicates a maximum distortion of the position as compared to other compounds.

The signal from the  $\text{Rb}_2\text{KFeF}_6$  elpasolite (Fig. 8) did not give new information about defects.

By comparing the experimental and calculated temperature dependences of the heat capacity of the  $\text{Rb}_2\text{KScF}_6$  single crystal (Fig. 9), we revealed an increase in the free energy, which is explained by point defects found in the crystal. Based on this fact, it is concluded that, in the  $\text{Rb}_2\text{KScF}_6$  elpasolite, surface defects dominate.

## 6. CONCLUSIONS

According to the EPR data,  $\text{ScF}_3$  single crystals (including the doped crystals), as well as a number of more complex compounds with the elpasolite structure, contain point defects occupied by electrons with the total spin  $S = 3/2$  and have a three-component structure of the EPR spectrum. These centers are characterized by a relatively high electron mobility, which made it possible using the additional hyperfine structure to reveal their location in fluorine octahedra and local distortions of these octahedra. The highest electron mobility is observed in  $\text{ScF}_3$  doped with iron. The largest distortion of the octahedral positions of defects is found in  $\text{Rb}_2\text{KDyF}_6$ . The second place is occupied by  $\text{ScF}_3$  doped with iron and  $\text{Rb}_2\text{KScF}_6$ . The disappearance of the EPR lines of defects in elpasolites after the exposure to air clearly indicates that these defects have a surface nature. In the  $\text{Rb}_2\text{KFeF}_6$  single crystal with an excess of iron, there also exist  $R$ -centers related to defects (Fig. 11). The Gibbs free energy was calculated using the experimental temperature dependence of the heat capacity of the

$\text{Rb}_2\text{KScF}_6$  single crystal. A comparison of the experimental temperature dependences of the heat capacity of the  $\text{Rb}_2\text{KFeF}_6$  single crystal and the calculated dependence (Fig. 9) revealed an increase in the free energy upon introduction of defects into the crystal. On this basis, it was concluded that surface defects dominate in the  $\text{Rb}_2\text{KScF}_6$  elpasolite.

It should be noted that the  $\text{ScF}_3$  crystals grown using a different method (from melt) by D.N. Karimov (Shubnikov Institute of Crystallography of the Russian Academy of Sciences, Moscow, Russia), for which we are very grateful to him, contain the same defect centers as those observed in our crystal.

## ACKNOWLEDGMENTS

This study was supported by the Council on Grants from the President of the Russian Federation (grant no. NSh 4828.2012.2).

## REFERENCES

1. H. G. Van Bueren, *Imperfections in Crystals* (North-Holland, Amsterdam, 1960; Mir, Moscow, 1962).
2. A. Kelly and G. Groves, *Crystallography and Crystal Defects* (Longman, Bristol, 1970; Mir, Moscow, 1974).
3. G. K. Wertheim, A. Hausmann, and W. Sander, *The Electronic Structure of Point Defects* (North-Holland, Amsterdam, 1971; Atomizdat, Moscow, 1977).
4. L. F. Mollenauer, S. Pan, and S. Yngresson, *Phys. Rev. Lett.* **23**, 683 (1969).
5. H. Seidel, *Phys. Lett.* **7**, 27 (1963).
6. H. Pick, *Z. Phys.* **159**, 69 (1960).
7. C. Z. Van Doorn and Y. Haven, *Philos. Res. Rep.* **11**, 419 (1956).
8. A. M. Stoneham, *Theory of Defects in Solids* (Clarendon, Oxford, 1975; Mir, Moscow, 1978), Vol. 1.
9. A. E. Hughes and B. Henderson, *Point Defects in Solids* (Plenum, New York, 1972), Vol. 1.
10. W. D. Compton and H. Rabin, *Solid State Phys.* **16**, 121 (1964).
11. W. Kanzig, *Phys. Rev.* **99**, 1890 (1955).
12. W. Ulrici, *Phys. Status Solidi B* **40**, 557 (1970).
13. J. H. Beament, W. Hayes, W. D. L. Kirk, and G. P. Summers, *Solid State Commun.* **6**, 903 (1968).
14. T. P. P. Hall, *Br. J. Appl. Phys.* **17**, 1011 (1966).
15. J. Arends, *Phys. Status Solidi B* **7**, 805 (1964).
16. K. S. Aleksandrov, V. N. Voronov, A. N. Vtyurin, S. V. Goryainov, N. G. Zamkova, V. I. Zinenko, and A. S. Krylov, *JETP* **94** (5), 977 (2002).
17. I. N. Flerov, R. Burriel, M. V. Gorev, P. Isla, and V. N. Voronov, *Phys. Solid State* **45** (1), 167 (2003).
18. E. G. Maksimov, V. I. Zinenko, and N. G. Zamkova, *Phys.—Usp.* **47** (11), 1075 (2004).
19. S. A. Al'tshuler and B. M. Kozyrev, *Electron Paramagnetic Resonance in Compounds of Transition Elements* (Nauka, Moscow, 1972; Wiley, New York, 1974).

Translated by O. Borovik-Romanova